

SATB2 Is a Multifunctional Determinant of Craniofacial Patterning and Osteoblast Differentiation

Gergana Dobрева,¹ Maria Chahrour,² Marcel Dautzenberg,¹ Laura Chirivella,³ Benoit Kanzler,¹ Isabel Fariñas,³ Gerard Karsenty,² and Rudolf Grosschedl^{1,*}

¹Max-Planck Institute of Immunobiology, Department of Cellular and Molecular Immunology, 79108 Freiburg, Germany

²Baylor College of Medicine, Department of Molecular and Human Genetics, Houston, TX 77030, USA

³Departamento de Biología Celular, Unidad Mixta CIPF-UVEG, Universidad de Valencia, 46100 Burjassot, Spain

*Contact: grosschedl@immunbio.mpg.de

DOI 10.1016/j.cell.2006.05.012

SUMMARY

Vertebrate skeletogenesis involves two processes, skeletal patterning and osteoblast differentiation. Here, we show that *Satb2*, encoding a nuclear matrix protein, is expressed in branchial arches and in cells of the osteoblast lineage. *Satb2*^{-/-} mice exhibit both craniofacial abnormalities that resemble those observed in humans carrying a translocation in *SATB2* and defects in osteoblast differentiation and function. Multiple osteoblast-specific genes were identified as targets positively regulated by SATB2. In addition, SATB2 was found to repress the expression of several *Hox* genes including *Hoxa2*, an inhibitor of bone formation and regulator of branchial arch patterning. Molecular analysis revealed that SATB2 directly interacts with and enhances the activity of both Runx2 and ATF4, transcription factors that regulate osteoblast differentiation. This synergy was genetically confirmed by bone formation defects in *Satb2/Runx2* and *Satb2/Atf4* double heterozygous mice. Thus, SATB2 acts as a molecular node in a transcriptional network regulating skeletal development and osteoblast differentiation.

INTRODUCTION

Skeletal development is initiated when mesenchymal cells aggregate at the location of and condense in the shape of future skeletal elements. These events, referred to as skeletal patterning, occur at various times throughout development of the skeleton and are controlled by major developmental signaling pathways and regulators of positional identity (Mariani and Martin, 2003). During craniofacial development, neural crest cells migrate ventrolaterally from specific segmented regions of the

hindbrain, termed rhombomeres, into the branchial arches to form specific components of the jaw apparatus (Hunt and Krumlauf, 1991; Bronner-Fraser, 1993; Köntges and Lumsden, 1996; Graham and Smith, 2001; Depew et al., 2002). Key players in these patterning events are, among others, *Hox* proteins, which confer anterior-posterior positional identity, and *Dlx5* and *-6*, which regulate dorsoventral patterning (Trainor and Krumlauf, 2001; Depew et al., 2002; Santagati and Rijli, 2003). Targeted inactivation of rhombomere-specific *Hox* genes and grafting experiments of neural crest cells indicate that patterning involves both segment-restricted *Hox* gene expression and interactions of migrating neural crest cells with the respective branchial arch environment (Chiaska et al., 1992; Gendron-Maguire et al., 1993; Rijli et al., 1993; Veitch et al., 1999).

The second important event during skeletal development is the differentiation of cells of various origins into three specialized cell types: mesenchymal cartilage-forming chondrocytes and bone-forming osteoblasts as well as myelomonocytic bone-degrading osteoclasts. Few skeletal elements, including parts of the skull, are generated by direct differentiation of mesenchymal progenitor cells into bone-forming osteoblasts in a process termed intramembraneous ossification; most bones are formed by endochondral ossification via a cartilaginous template (Olsen, et al., 2000; de Crombrughe et al., 2001). Differentiation along the osteoblast lineage has been shown to depend on three transcriptional regulators. *Runx2* and *Osterix* are both required for the early and late stages of osteoblast differentiation, whereby *Runx2* is a master regulator that acts upstream of *Osterix* (Nakashima et al., 2002). In addition, *Atf4* regulates the terminal differentiation and function of osteoblasts, including the synthesis of the most abundant bone extracellular matrix protein, Type I collagen (Yang et al., 2004).

The function of various transcription factors and *cis*-acting sequences can be regulated by proteins that are part of the nuclear matrix and bind AT-rich sequences, referred to as nuclear matrix-attachment regions (MARs; Bode et al., 2000). MAR sequences and MAR binding proteins have been implicated in the higher-order organization of

chromatin and in the regulation of long-range interactions between enhancers and promoters (Cockerill and Garrard, 1986; Gasser and Laemmli, 1986; Jenuwein et al., 1997). Several transcription factors, including Runx2, have been shown to associate with the nuclear matrix, and these associations have been implicated in the sub-nuclear localization and function of these transcription factors (Zaidi et al., 2005).

SATB2 is a recently cloned member of the family of special AT-rich binding proteins that binds to MARs and activates transcription in a MAR-dependent manner (Dobrev et al., 2003; Britanova et al., 2005). In humans, translocations that involve the chromosomal region 2q32-q33 and are associated with a cleft palate under conditions of haploinsufficiency have been found to interrupt the *SATB2* gene (FitzPatrick et al., 2003). SATB2 is closely related to the thymocyte-specific SATB1 protein (Kohwi-Shigematsu et al., 1997). SATB1 regulates multiple genes and has been found to act as a repressor of transcription by recruiting the Sin3a histone deacetylase and subunits of the ACF nucleosome-mobilizing complex to target genes (Alvarez et al., 2000; Yasui et al., 2002). In addition, SATB1 has been proposed to act by tethering MAR sequences onto its "cage-like" proteinaceous scaffold (Cai et al., 2003).

Here, we analyze the function of SATB2 in skeletogenesis. We find that SATB2 represses the expression of *Hoxa2* and activates several osteoblast-specific genes by augmenting the activity of both Runx2 and ATF4, suggesting that SATB2 acts as a molecular node in a transcriptional network regulating skeletogenesis.

RESULTS

Generation of *Satb2* Knockout Mice and Analysis of *Satb2* Expression in Development

To gain insight into the physiological role of SATB2, we inactivated the *Satb2* gene in mouse embryonic stem (ES) cells by homologous recombination and in-frame insertion of the bacterial β -galactosidase (*LacZ*) gene immediately downstream of the first ATG codon in exon 2 (Figure S1A). Mice carrying a mutant *Satb2-LacZ* allele were mated to generate heterozygous and homozygous mutant mice (Figure S1B; data not shown). Immunoblot analysis of fetal brain tissue using anti-SATB2 and anti- β -Gal antibodies indicated that β -galactosidase protein, but not SATB2 protein, is detected in *Satb2*^{-/-} mice (Figure S1C). Thus, the targeted gene inactivation generated a null mutation of the *Satb2* gene.

We examined the developmental expression pattern of *Satb2* by analyzing the presence of β -galactosidase activity in heterozygous *Satb2*^{+/-} mice between E8.5 and E14.5 (Figures 1A and 1B). Whole-mount staining for β -galactosidase activity revealed expression in the rhombomere region of the hindbrain at E8.5 and in the first branchial arch at E9. In addition, β -galactosidase activity was found in the hindgut diverticulum of E9 embryos. At E10.5, *LacZ* expression was detected in all four branchial

arches, in the apical ectodermal ridge (AER), and in the zone of polarizing activity of the limb buds. Coronal sections indicated that *LacZ* expression is restricted to the medial portion of the branchial arches (Figure 1A). At E12.5 and E14.5, we detected abundant *LacZ* expression in the cortex of the brain and at sites of bone formation (Figure 1B). Additional *LacZ* expression was found in the spinal cord, kidneys, and the umbilical cord. We also confirmed by in situ hybridization that the pattern of *LacZ* expression in E15.5 and E16.5 *Satb2*^{+/-} embryos is virtually identical to that of endogenous *Satb2* transcription in corresponding wild-type embryos (Figures 1C and 1D).

Perinatal Lethality, Cleft Palate, and Skeletal Patterning Defects in *Satb2*^{-/-} Mice

Heterozygous *Satb2*^{+/-} mice are phenotypically normal and fertile. Homozygous mutant mice can be obtained with the expected Mendelian frequency; however, they die immediately after birth. Until E12.5, *Satb2*^{-/-} mice show no obvious morphological abnormalities, but starting at E14.5, the mutants can be easily recognized by a shorter lower jaw (Figure S1D). Alcian Blue/Alizarin Red staining of skeletal preparations of E17.5 embryos confirmed that the homozygous mutants have a shortened mandible and alterations of several intramembraneous bones that are derived from the first branchial arch (premaxilla, maxilla, nasal bones, frontal bones, and temporal processes of the squamous bone; Figures 1E and 1F). Moreover, various skeletal elements that are derived from the second and third branchial arches, including the lesser horns and the body of the hyoid bone, are malformed (Figure 1F). In particular, the lesser horns are fused and show no articulation. The thyroid cartilage is missing from the laryngeal cartilages, whereas the arytenoid, cricoid cartilages and the tracheal rings, derivatives of more caudal branchial arches, are normal (Figure 1F). The skeletal elements of the middle ear are also normal in the mutant mice (data not shown).

SATB2 is expressed in the mandibular component of the first branchial arch, which gives rise to the lower jaw (Köntges and Lumsden, 1996; Fitzpatrick et al., 2003). Histological analysis of the mandible of E18.5 heads in horizontal sections indicated that the posterior half of the homozygous mutant mandible appeared normally shaped and contained Meckel's cartilage and developing molar teeth (Figure 2A). In contrast, the anterior part of the mandible, which contains normally the lower incisors and the anterior fusion of the Meckel's cartilage, is missing in the mutant mandible (Figure 2A). The incisor teeth, which express high levels of SATB2 in wild-type embryos, are missing in E17.5 *Satb2*^{-/-} embryos, although developing tooth germs can be detected at E13.5 (Figures 2B, S1E, S1F, S1H, and S1I). The molars, which do not express SATB2, are unaffected in homozygous mutant embryos (Figures S1G, S1J, and S1K).

Based on the association of a mutation in the human SATB2 locus with a cleft palate (FitzPatrick et al., 2003), we examined coronal sections of heads of E17.5 embryos. *Satb2*^{-/-} embryos show a cleft palate and a significantly

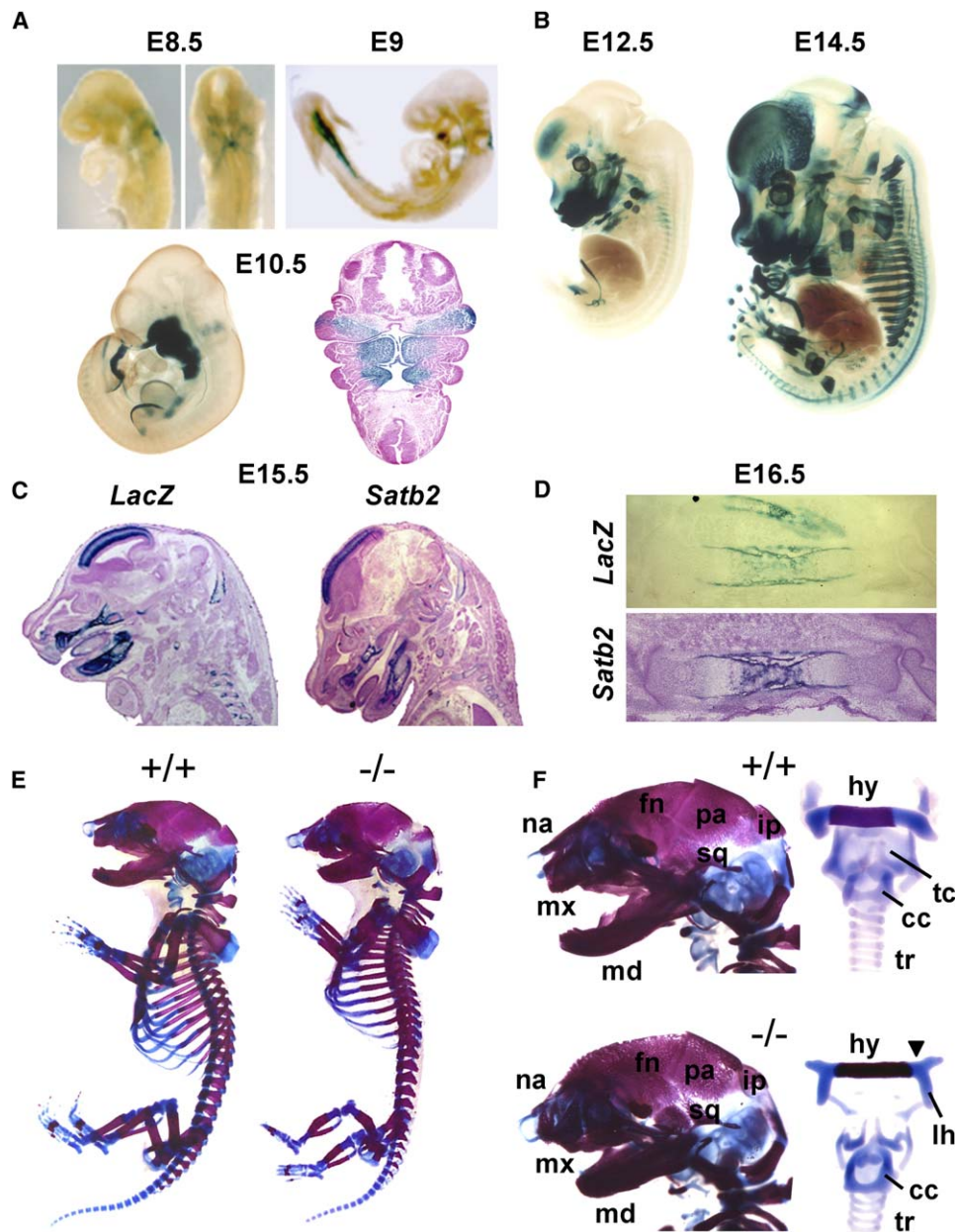


Figure 1. Developmental Expression Pattern of *Satb2* and Skeletal Abnormalities in *Satb2*^{−/−} Mice

(A) β -galactosidase staining of E8.5–E10.5 *Satb2*^{+/−} embryos to detect SATB2-LacZ expression in whole mounts and in a coronal section through an E10.5 embryo.

(B) Whole-mount β -galactosidase staining of E12.5 and E14.5 *Satb2*^{+/−} embryos shows LacZ expression in the developing skeleton.

(C and D) In situ hybridization to detect *Satb2* transcripts and β -galactosidase staining to detect LacZ expression in sagittal sections of E15.5 *Satb2*^{+/−} embryos (C) and E16.5 tibias (D), showing virtually identical *Satb2* and LacZ expression pattern.

(E) Skeletal preparations of E17.5 wild-type (+/+) and mutant (−/−) embryos, showing craniofacial malformations and shortening of the hindlimbs.

(F) Magnified view of E17.5 heads (left-hand) and dissected hyoid bone and laryngeal cartilages (right-hand). The mandible (md) and maxilla (mx) are shortened in the mutants. The lesser horns (lh) and the body of the hyoid bone (hy) are malformed, and the thyroid cartilage (tc) is absent in the mutant. fn, frontal bone; na, nasal bone; pa, parietal bone; ip, interparietal bone; sq, squamous bone; cc, cricoid cartilage; tr, tracheal rings.

smaller and shorter tongue, relative to wild-type embryos (Figures 2B, S1H, and S1J). Scanning electron microscopy of the oral cavity roof at E14.5 suggested that the cleft palate defect in the *Satb2*^{−/−} embryos may be the re-

sult of a failure in the midline fusion of the palatal shelves and the drop-down of the tongue (Figure 2C). TUNEL assays to assess apoptosis and immunohistochemistry to detect both SATB2-LacZ expression, and BrdU

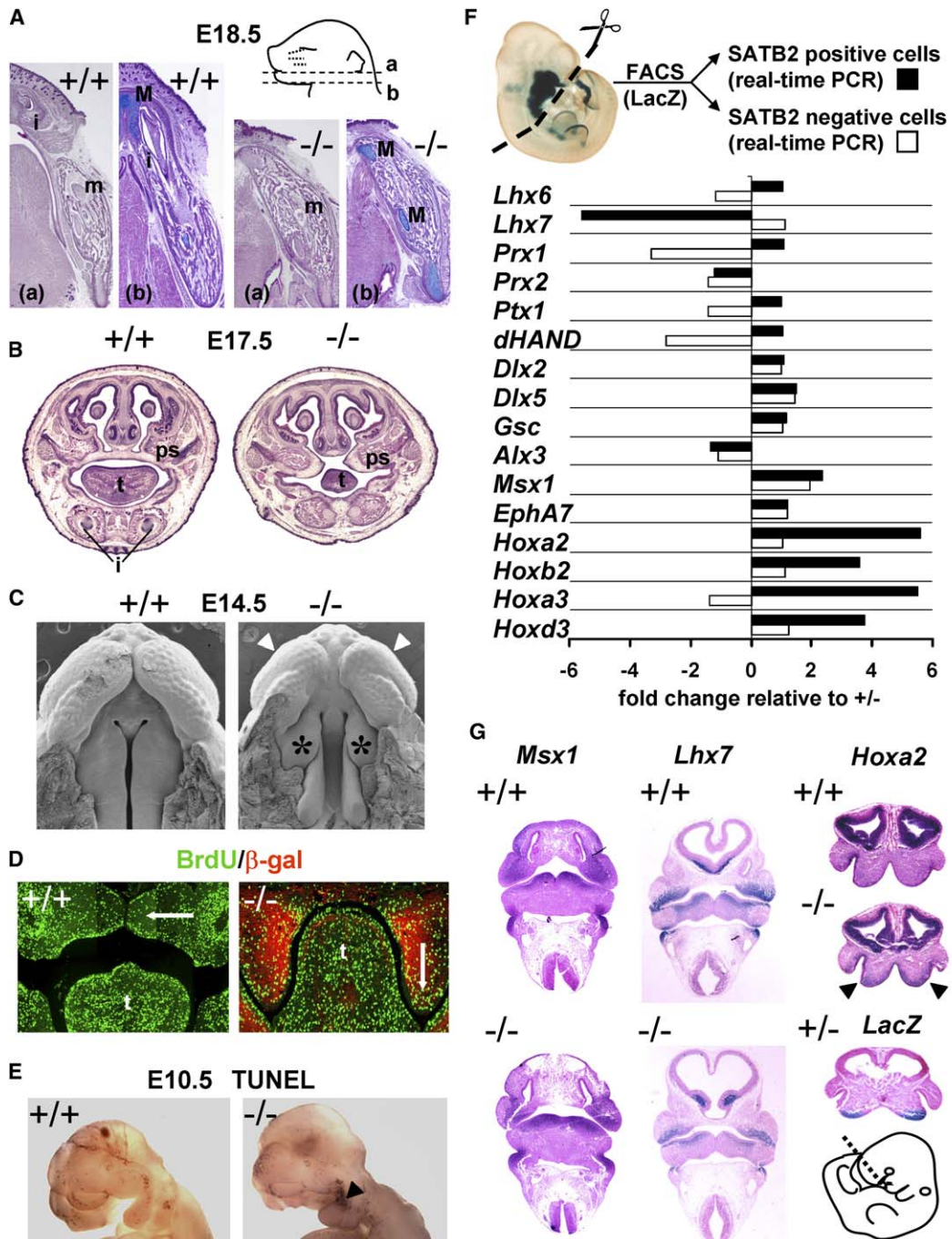


Figure 2. Patterning Defects in SATB2-Deficient Mice

(A) Horizontal sections through the lower jaws of wild-type (+/+) and *Satb2* mutant (−/−) E18.5 embryos at two different planes, separated by 300 μm and stained with hematoxylin-eosin alone (a) or together with alcian blue (b). M, Meckel’s cartilage; m, molar tooth; i, incisor tooth.

(B) Coronal sections of E17.5 wild-type and *Satb2*^{−/−} heads showing a cleft palate and the absence of incisors (i). ps, palatal shelves; t, tongue.

(C) Scanning electron micrographs of heads of E14.5 embryos. The palatal shelves of *Satb2*^{−/−} embryos fail to grow toward the fusion line (asterisks), and the maxillary processes do not converge at the tip of the snout (arrowheads).

(D) BrdU incorporation (green) and β-galactosidase immunohistochemistry (red) in E14.5 embryos show normal proliferation of the SATB2-LacZ-positive mesenchyme of *Satb2*^{−/−} palatal shelves. White arrows indicate the direction of the maxillary processes.

(E) Whole-mount TUNEL assays on E10.5 embryos showing increased apoptosis in the first branchial arch of *Satb2*^{−/−} embryos (arrowhead).

(F) Quantitative RT-PCR analysis on SATB2-LacZ-expressing cells (dark bars) that have been isolated by flow cytometry from dissected head and branchial arch regions of *Satb2*^{−/−} and *Satb2*^{+/−} embryos. Expression levels of candidate target genes in *Satb2*^{−/−} cells, normalized to β-actin, are presented relative to the expression levels in the *Satb2*^{+/−} cells. As a control, SATB2-LacZ-nonexpressing cells (open bars) were used.

incorporation indicated that cell proliferation and survival are normal in the β -Gal-positive mesenchyme of the mutant palatal shelves (Figures 2D and S2A). However, the *Satb2*^{-/-} palatal shelf mesenchyme generates bulges not observed in wild-type mice (Figure 2C), suggesting that the cleft palate may be caused by a patterning defect. We also examined whether phenotypic changes can be detected at earlier stages of development and observed enhanced apoptosis in the first branchial arch of E10.5 SATB2-deficient embryos (Figure 2E).

To gain insight into potential mechanisms underlying the craniofacial defects, we examined the expression of candidate genes that have been implicated in the patterning of branchial arch-derived structures. We performed quantitative RT-PCR with RNA isolated from cells in the head and branchial arch regions of E10.5 *Satb2*^{+/-} and *Satb2*^{-/-} embryos that have been loaded with the fluorogenic β -galactosidase substrate FDG and sorted by flow cytometry. As a control, we used cells that were negative for SATB2-LacZ expression. We failed to detect changes in the expression of *Dlx5*, *Dlx6*, *Ptx1*, *Prx1*, *Prx2*, *dHand*, and *EphA7* (Figure 2F). However, we detected a 5-fold decrease in the level of *Lhx7* expression and 4- to 6-fold increases in the expression of several *Hox* genes. In situ hybridizations to detect transcripts of *Dlx1*, *Dlx2*, *Gsc*, *Ptx1*, *Alx3*, and *Msx2* did not reveal any obvious differences between wild-type and *Satb2*^{-/-} embryos; however, the expression domain of *Msx1* is reproducibly extended in the mandible of E11.5 mutant embryos (Figures 2G and S2C–S2F; data not shown). Moreover, the expression of *Lhx7* was decreased, consistent with the quantitative RT-PCR analysis (Figure 2G). The expression of *Hoxa2* in the branchial arches was found to be relatively normal, although an upregulation was detected in the fronto-nasal processes (Figure 2G).

Defects of Osteoblast Differentiation in *Satb2*^{-/-} Mice

In addition to the craniofacial patterning defects, skeletal preparations of E15.5 *Satb2*^{-/-} embryos showed delayed bone formation or mineralization, as assessed by Alizarin Red-staining (Figure S3A). Staining of developing long bones with a van Gieson dye that labels collagen fibers showed that collagen levels are markedly reduced in E14.5 mutant compared to wild-type embryos, a difference even more pronounced in E15.5 embryos (Figures 3A and 3B). Electron microscopy analysis showed a virtual absence of osteoid seams in the trabeculae of *Satb2*^{-/-} developing bones, suggesting a defect in extracellular matrix deposition (Figure S3H). X-gal staining of long bones of *Satb2*^{+/-} mice at E17.5 showed that SATB2 is expressed in the osteoblast lineage but not in chondrocytes (Figure 3C). Moreover, immunostaining of wild-type bones for SATB2 and costaining to detect tartrate-

resistant alkaline phosphatase-expressing osteoclasts indicated that SATB2 is not expressed in osteoclasts (Figure S3E).

Analysis of molecular markers for osteoblast differentiation indicated that expression of *Osterix* (*Osx*) and *alkaline phosphatase* (*AP*) is reduced in long bones of E14.5 *Satb2*^{-/-} embryos (Figure 3A). Von Kossa staining to detect mineral deposits showed that the trabeculae of the homozygous mutant bone are shorter and thinner than those of the wild-type bone, whereas the growth plate is normal (Figures 3D and S3F). Von Kossa staining and quantitative micro-CT of vertebrae confirmed the marked defect in the formation of trabeculae and bone volume (Figures 3E and 3F). We also examined the expression of *bone sialoprotein* (*Bsp*), an early marker for osteoblast differentiation, and *osteocalcin* (*Ocn*), a marker for terminal osteoblast differentiation, by in situ hybridization. Both markers were downregulated in long bones and calvariae of *Satb2*^{-/-} embryos (Figures 3D and S3D; data not shown). Quantification of the changes in the expression of these and other genes by real-time RT-PCR with RNA from calvarial osteoblasts indicated that *Ocn* and *Bsp* expression is reduced in the mutant cells 43-fold and 5-fold, respectively (Figure 3G). No change of *Osterix* expression was detected, whereas the expression of *Runx2*, *Atf4*, *Dlx3*, and *Dlx5* was only modestly decreased (Figure 3G). Finally, we analyzed in cell culture the ability of *Satb2*^{-/-} osteoblasts to differentiate into cells able to produce and mineralize an extracellular matrix. The percentage of bone nodules in *Satb2*^{-/-} osteoblasts was reduced 5-fold relative to wild-type and heterozygous osteoblasts, whereas cell proliferation was not altered (Figure S4A; data not shown). This defect was not rescued by the addition of bone morphogenetic protein-2 (BMP2), which induces the expression of both *Runx2* and *Satb2* in wild-type osteoblasts (Figures S4A and S4B).

SATB2 Regulates Multiple Genes in Osteoblasts and Represses *Hoxa2* Expression

To gain insight into the role of SATB2 in osteoblasts, we performed gene expression profiling by hybridizing RNA from *Satb2*^{+/-} and *Satb2*^{-/-} calvarial osteoblasts that had been sorted for *LacZ* expression. The microarray analysis was performed on pools of five to six mice and showed that the expression of multiple genes, encoding transcription factors, extracellular matrix proteins, and growth factors are consistently deregulated in SATB2-deficient osteoblasts (Figure 4A). Consistent with the quantitative RT-PCR analysis of osteoblast cultures, expression of *Bsp* was markedly downregulated, whereas the expression of chondrocyte-specific extracellular matrix proteins (*Collagen2a1*, *Collagen9a1*, *Matrilin*, and *Elastin*) and chondrocyte-specific transcription factors (*Sox5* and *Sox6*) were found to be upregulated. These changes in gene

(G) In situ hybridization on transverse sections of E11.5 wild-type and *Satb2*^{-/-} embryos to detect *Msx1* and *Lhx7* transcripts (left-hand and middle). In situ hybridization to detect *Hoxa2* transcripts in coronal sections of E10.5 embryos (right-hand) shows ectopic *Hoxa2* expression in the frontonasal processes (arrowheads; the section level is indicated at the bottom).

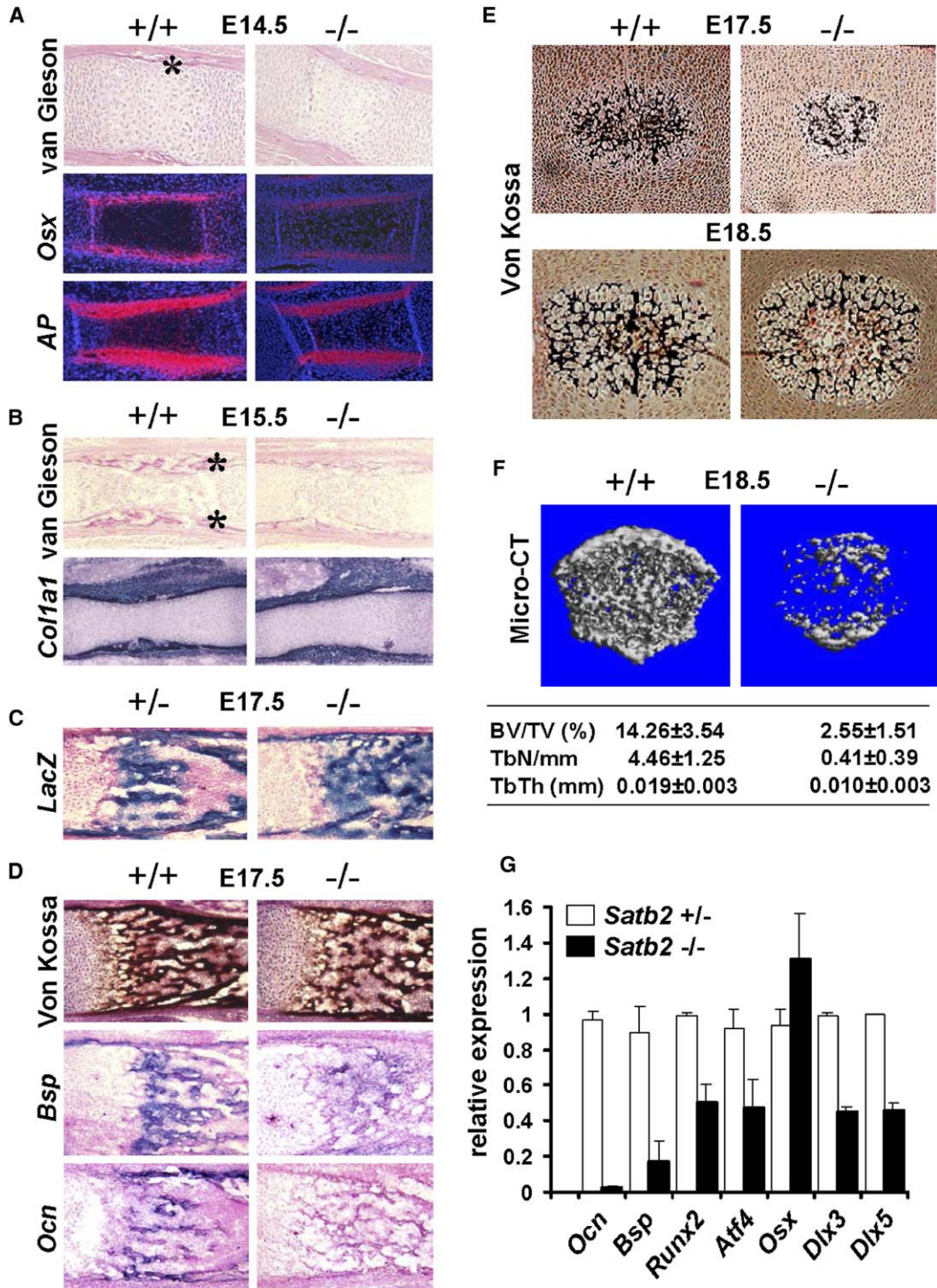


Figure 3. Analysis of Bone Defects in SATB2-Deficient Mice

(A) Van Gieson staining to detect collagen fibers (asterisk) and in situ hybridization to detect transcripts of Osterix (*Osx*) and alkaline phosphatase (*AP*) show the absence of collagen fibers and downregulation of *Osx* and *Ap* in E14.5 *Satb2*^{-/-} long bones.

(B) Van Gieson staining and in situ hybridizations to detect transcripts of Collagen1a1 (*Col1a1*) in E15.5 long bones show the absence of trabeculae in the mutant (upper panels).

(C) β-galactosidase staining on cryosections of tibias from E17.5 embryos shows SATB2-LacZ expression in osteoblasts.

(D) Von Kossa staining of mineralized extracellular matrix and in situ hybridizations to detect transcripts of bone sialoprotein (*Bsp*) and osteocalcin (*Ocn*) in E17.5 tibias.

expression suggest that the SATB2-deficient osteoblasts have a more immature phenotype, consistent with their inability to fully differentiate when cultured in vitro (Figure S4A). Notably, we also found a downregulation of *Lhx7* expression and an upregulation of *Hoxa2*, which is also deregulated in the fronto-nasal region of *Satb2*^{-/-} embryos.

In addition to its role in craniofacial patterning, *Hoxa2* has been shown to antagonize bone formation (Kanzler et al., 1998). Consistent with these data, in situ hybridizations on coronal sections of E15.5 heads showed a marked upregulation of *Hoxa2* expression in areas of SATB2-deficient calvarial bones that express SATB2-LacZ (Figures 4B and S3C). To confirm this result, we performed quantitative RT-PCR analysis on sorted *LacZ*-expressing primary osteoblasts and found that *Satb2*^{-/-} osteoblasts contained ten times more *Hoxa2* transcripts than *Satb2*^{+/-} cells (Figure 4C). The level of *Hoxa2* expression was reduced 4-fold in *Satb2*^{-/-} osteoblasts that have been transduced with a retrovirus expressing SATB2.

The regulation of *Hoxa2* gene expression has been analyzed in detail and shown to depend on a set of enhancers that control its expression in different tissues (Tumpel et al., 2002). In particular, the intragenic E1 enhancer and the downstream E11 enhancer were found to determine *Hoxa2* expression in rhombomeres 4 and 2, respectively (Figure 4D; Frasch et al., 1995). In silico analysis of the *Hoxa2* enhancer sequences by the MAR-Wiz algorithm identified a putative MAR element within the E11 enhancer (Namciu et al., 2004; data not shown). To examine the binding of SATB2 to these regulatory elements in vivo, we infected primary osteoblasts with a retrovirus expressing FLAG-SATB2 and performed chromatin immunoprecipitation (ChIP) using an anti-FLAG antibody (Figure 4E). The immunoprecipitated chromatin fragments were analyzed with multiple primer pairs that allow for the amplification of different regions of the *Hoxa2* enhancers. SATB2 was found to be bound to this region of the E11 enhancer but not to the E1 enhancer in vivo (Figure 4E). Moreover, binding to the E11 enhancer appears to be direct, as recombinant SATB2 can efficiently bind to an oligonucleotide encompassing sequences of the E11 enhancer in an electrophoretic mobility shift assay (Figure S4C, left-hand). Finally, the expression of SATB2 was found to result in a 3- to 5-fold decrease in K4 methylation of histone H3 at the endogenous *Hoxa2* gene (Figure S4C, right-hand).

To assess the regulation of the E11 enhancer by SATB2, we transfected an E11 enhancer-luciferase gene construct into *Satb2*^{+/-} and *Satb2*^{-/-} osteoblasts. The activity of the E11 enhancer was increased 4-fold in *Satb2*^{-/-} osteoblasts relative to *Satb2*^{+/-} cells, whereas the enhancer-less re-

porter gene was expressed at similar high levels (Figure 4F). We also examined the effect of the deletion of the SATB2 binding region in the context of a transgene, in which a *LacZ* gene has been inserted into the *Hoxa1* gene downstream of the E11 enhancer (Frasch et al., 1995). Deletion of the MAR resulted in some embryos in an ectopic expression in the cortex and AER of the limb buds, sites that normally express SATB2 (Figures 1A and S4D).

To obtain genetic evidence for the repression of *Hoxa2* by SATB2 in osteoblasts, we examined whether the delay of calvarial bone formation in *Satb2*^{-/-} embryos can be overcome by inactivation of the *Hoxa2* gene. To this end, we mated *Satb2*^{+/-} mice with *Hoxa2*^{+/-} mice and analyzed compound homozygotes at E18.5. Consistent with the upregulation of *Hoxa2* in the calvariae of *Satb2*^{-/-} embryos, we found that the delay in calvarial bone formation of *Satb2*^{-/-} embryos is largely rescued in *Satb2*^{-/-}*Hoxa2*^{-/-} mice (Figure 4G). Taken together, these data indicate that the repression of *Hoxa2* in calvarial osteoblasts by binding of SATB2 to the E11 enhancer is important for normal osteoblast differentiation.

SATB2 Binds to and Regulates the Bone Sialoprotein and Osteocalcin Promoters

To assess the role of SATB2 in the regulation of *Bsp* and *Ocn*, we performed quantitative RT-PCR with RNA from primary osteoblasts that had been sorted for *LacZ* expression and cultured in vitro. In *Satb2*^{-/-} cells, we detected a 12-fold and 6-fold downregulation of *Bsp* and *Ocn*, respectively, whereas the expression of these genes was increased to normal levels in *Satb2*^{-/-} cells that had been transduced with a SATB2-expressing retrovirus (Figure 5A). Previous studies of the *bone sialoprotein* (*Bsp*) promoter have identified three regulatory sequence elements in a region between -290 and -181 that determine osteoblast-specific promoter activity (Figure 5B; Benson et al., 2000). ChIP analysis of wild-type osteoblasts that had been infected with a retrovirus expressing FLAG-tagged SATB2 showed binding of SATB2 to *Bsp* sequences that include the three osteoblast-specific sequence elements (Figure 5B, lower panel). No binding of SATB2 was detected with primers that amplify an upstream *Bsp* promoter region. In an EMSA we found that recombinant SATB2 efficiently bound to a *Bsp* oligonucleotide encompassing the wild-type site C but not to an oligonucleotide carrying mutations that have been previously shown to impair *Bsp* promoter activity (Figure 5D, left-hand; Benson et al., 2000).

The *Ocn* promoter has been extensively studied and shown to be regulated by Runx2 and ATF4, which bind the nonadjacent sequence elements OSE2 and OSE1,

(E) Von Kossa staining in vertebrae sections of wild-type and *Satb2*^{-/-} embryos at E17.5 and E18.5.

(F) Micro-CT analysis of P0 wild-type and *Satb2*^{-/-} vertebrae. Note the decrease in bone volume/ total bone volume (BV/TV), trabeculae number per mm (TbN/mm), and trabecular thickness (TbTh) in *Satb2*^{-/-} mice.

(G) Quantitative RT-PCR analysis to determine the relative expression levels of osteoblast-specific genes in *Satb2*^{+/-} and *Satb2*^{-/-} osteoblasts, sorted for *LacZ* expression without in vitro culture. Error bars represent the standard deviation of four experiments.

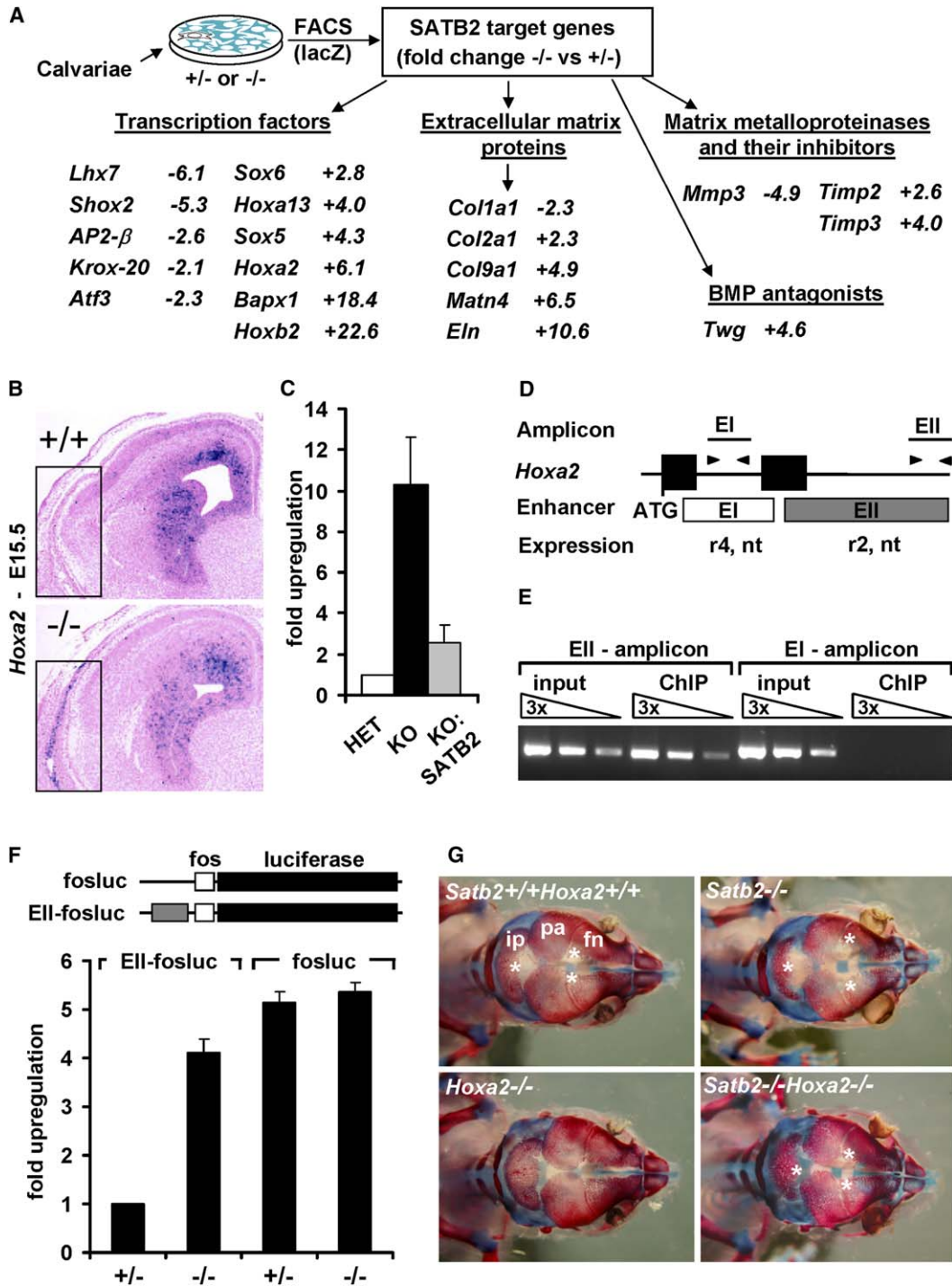


Figure 4. Identification of SATB2 Target Genes and Regulation of *Hoxa2* Expression by SATB2

(A) Affymetrix GeneChip array analysis of *Satb2*^{+/-} and *Satb2*^{-/-} osteoblasts sorted for *LacZ* expression. The fold changes in transcript levels in *Satb2*^{-/-} cells, relative to *Satb2*^{+/-} cells, are indicated.

(B) In situ hybridization of E15.5 heads (one hemisphere is shown) reveals ectopic expression of *Hoxa2* in *Satb2*^{-/-} calvariae (boxed area).

(C) Quantitative RT-PCR analysis detects an upregulation of *Hoxa2* expression in *Satb2*^{-/-} osteoblasts but not in mutant cells that have been transduced with a SATB2-expressing retrovirus 48 hr prior to the analysis. The levels of gene expression in *Satb2*^{-/-} osteoblasts (black bars) and *Satb2*^{-/-} transduced *Satb2*^{-/-} osteoblasts (gray bars) are presented relative to *Satb2*^{+/-} osteoblasts (white bars). The data are averages plus standard deviation of four independent experiments.

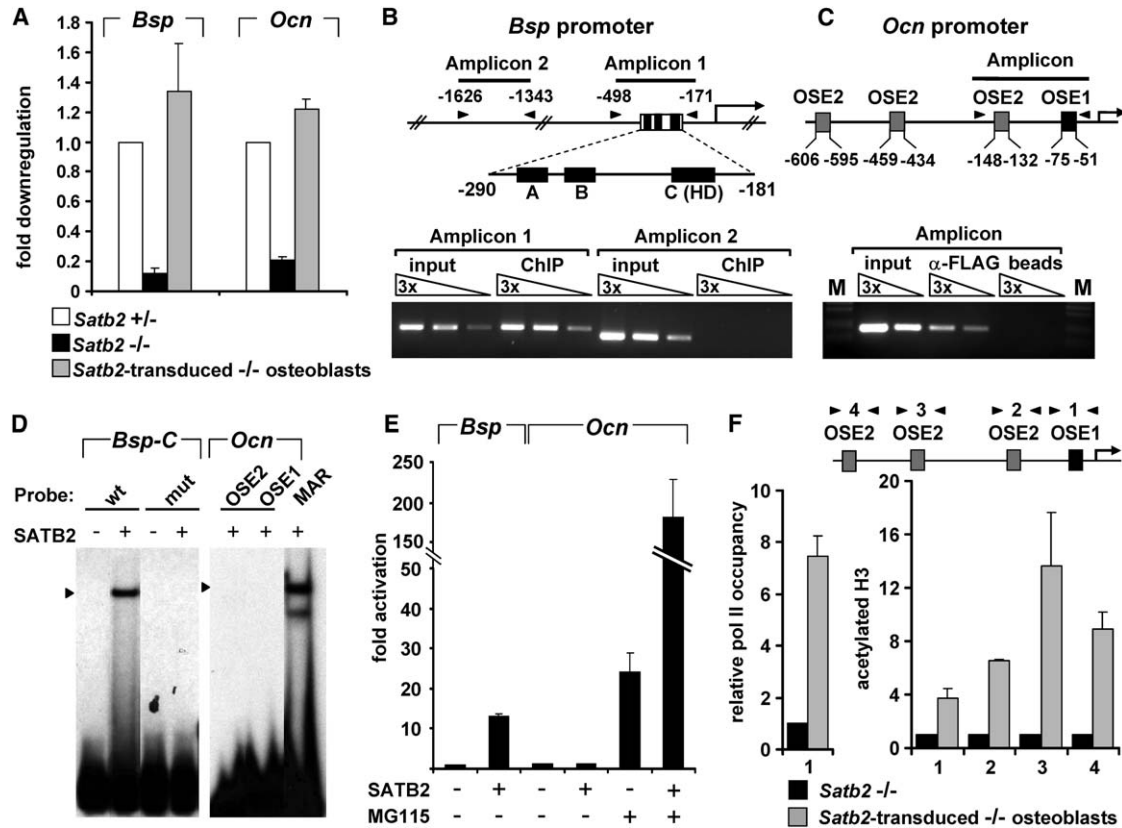


Figure 5. SATB2 Regulates the Expression of *Bsp* and *Ocn*

(A) Quantitative RT-PCR analysis of sorted SATB2-deficient osteoblasts that had been transduced with a *Satb2*-expressing retrovirus (gray bars) shows a reversal of *Bsp* and *Ocn* downregulation relative to *Satb2*^{+/+} cells (white bars). The data are averages plus standard deviation of four independent experiments.

(B) Detection of SATB2 binding to the *Bsp* promoter by ChIP analysis. Schematic representation of the regulatory elements in the *Bsp* promoter, including three osteoblast-specific elements, A–C (Benson et al., 2000; upper panel). ChIP on FLAG-SATB2 transduced osteoblasts detects specific binding of SATB2 to the *Bsp* promoter region.

(C) Schematic representation of the *Ocn* promoter showing the positions of the binding sites for ATF4 (OSE1) and Runx2 (OSE2) (upper panel). The ChIP analysis detected binding of FLAG-SATB2 to a promoter fragment containing OSE1 and OSE2.

(D) Electrophoretic mobility shift assay (EMSA) showing binding of purified recombinant SATB2 to wild-type (wt), but not mutated (mut), *Bsp* site C oligonucleotides (left panel). No SATB2 binding was detected to wild-type OSE1 and OSE2 oligonucleotides (right panel). The MAR consensus oligonucleotide was used as a positive control.

(E) Quantitative RT-PCR analysis to determine the levels of endogenous *Bsp* and *Ocn* expression in C2C12 cells that had been transduced with a SATB2- or GFP-expressing retrovirus. Cells were either untreated or treated with the proteasome inhibitor MG115. The data are averages plus standard deviation of four independent experiments.

(F) ChIP assay to detect changes in H3 acetylation and pol II occupancy at the *Ocn* promoter in *Satb2*^{-/-} (black bars) and *Satb2*-transduced *Satb2*^{-/-} osteoblasts (gray bars). Error bars represent the standard deviation of three experiments.

respectively (Figure 5C; Bidwell et al., 1993; Ducy and Karsenty, 1995; Yang et al., 2004). To determine whether SATB2 is bound to the *Ocn* promoter in vivo, we performed

ChIP experiments with primary wild-type osteoblasts that had been infected with a FLAG-SATB2-expressing retrovirus or a GFP-expressing control virus.

(D) Schematic representation of the *Hoxa2* gene and its regulatory sequences. The primer pairs used for the chromatin immunoprecipitation (ChIP) are shown as arrowheads.

(E) ChIP assay to detect SATB2 binding in primary osteoblasts that had been infected with a retrovirus expressing FLAG-*Satb2*. PCR products were amplified from 3-fold serial dilutions of anti-FLAG immunoprecipitated chromatin fragments.

(F) Analysis of E11 enhancer activity in sorted *Satb2*^{+/+} and *Satb2*^{-/-} osteoblasts that have been transfected with a fos-luciferase construct containing or lacking the *Hoxa2* E11 enhancer. Error bars represent the standard deviation of three experiments.

(G) Top view of Alizarin Red/ Alcian Blue-stained skulls of E18.5 wild-type, *Satb2*^{-/-}, *Hoxa2*^{-/-}, and *Satb2*^{-/-}*Hoxa2*^{-/-} embryos. The frontal (fn), parietal (pa), and interparietal (ip) bones are indicated. Bone formation is decreased in *Satb2*^{-/-}, and this defect is largely rescued (asterisks mark edges of the frontal and interparietal bones) in *Satb2*^{-/-}*Hoxa2*^{-/-} embryos.

Immunoprecipitation with anti-FLAG antibody and amplification with primers flanking the proximal OSE2 and OSE1 sequences indicated that SATB2 is bound to the endogenous *Ocn* promoter (Figure 5C, lower panel). However, we failed to identify putative MAR elements using the MAR-Wiz algorithm and were unable to detect binding of SATB2 to either OSE2 or OSE1 in an EMSA (Figure 5D, right-hand).

To obtain further evidence for a role of SATB2 in the regulation of *Bsp* and *Ocn*, we examined whether forced expression of SATB2 induces the expression of the endogenous genes. To this end, we infected C2C12 cells with a GFP- or SATB2-expressing retrovirus and analyzed *Bsp* and *Ocn* expression by quantitative RT-PCR. In SATB2-expressing cells, *Bsp* expression was increased 12-fold, whereas *Ocn* expression was not significantly altered (Figure 5E). Based on the noted similarity of the bone phenotype in *Satb2*^{-/-} and *Atf4*^{-/-} mice, we examined whether SATB2 could induce *Ocn* expression in combination with ATF4. We treated cells with the proteasome inhibitor MG115, which has been previously shown to stabilize ATF4 and Runx2 and increase *Ocn* expression (Yang and Karsenty, 2004). As anticipated, MG115 treatment augmented *Ocn* expression ~25-fold, and this activation was further enhanced by a factor of seven in SATB2-expressing cells (Figure 5E). Finally, we found that the forced expression of SATB2 in *Satb2*^{-/-} osteoblasts increased the acetylation of histone H3 and the RNA polymerase II occupancy of the *Ocn* promoter, relative to SATB2-deficient cells (Figure 5F).

Cooperation of SATB2 with Both ATF4 and Runx2

The augmentation of *Ocn* expression by SATB2 raised the question of whether SATB2 interacts functionally or physically with Runx2 and/or ATF4, the two key regulators of *Ocn*. To this end, we transfected transiently COS7 cells with an *Ocn*-luciferase reporter, alone or together, with various combinations of expression plasmids for SATB2, Runx2, and ATF4 (Figures 6A and S5). Individually, Runx2, but not SATB2 or ATF4, augmented the activity of the 647bp *Ocn* promoter fragment. However, SATB2 augmented the Runx2-mediated activation by a factor of three, and this stimulation was further enhanced by the co-expression of ATF4 (Figure 6A). To examine whether SATB2 directly stimulates the activation by ATF4 or Runx2, we used reporter plasmids that contain multimerized ATF4 binding sites (6xOSE1-luciferase; Figure 6B) or multimerized Runx2 binding sites (6xOSE2-luciferase; Figure 6C). SATB2 alone did not activate these reporters, but it augmented ATF4- and Runx2-mediated activation by factors of two and four, respectively (Figures 6B and 6C, black bars). As a control, SATB2 had no effect on reporters in which the ATF4- or Runx2 binding sites had been mutated (Figures 6B and 6C, white bars).

To delineate the domains of Runx2 and ATF4 that mediate the functional collaboration with SATB2, we transfected various deletion constructs of Runx2 and ATF4 together with a SATB2 expression plasmid. Deletion of

the 108 amino-terminal residues of Runx2 abrogated the collaboration with SATB2, whereas the other deletions impaired activation of the 6xOSE2 reporter but did not affect stimulation by SATB2 (Figure 6D). Likewise, deletion of the 199 amino-terminal residues of ATF4 impaired the collaboration with SATB2 (Figure 6E).

Finally, we determined the effects of SATB2 on DNA binding by ATF4 and Runx2. We performed an EMSA with nuclear extracts from Ros cells, which contain endogenous Runx2 and ATF4 and have been infected with a SATB2- or GFP-expressing retrovirus (Figure 6F). Binding of ATF4 to OSE1 and Runx2 to OSE2 was detected, and the identities of the protein:DNA complexes were confirmed by the addition of anti-ATF4 or anti-Runx2 antibodies. No effect was observed by the addition of an anti-fos antibody. In extracts containing SATB2, an enhancement of DNA binding by both ATF4 and Runx2 was detected but without the appearance of slower-migrating protein:DNA complexes (Figure 6F).

Physical and Genetic Interaction of SATB2 with ATF4 and Runx2

To gain further insight into the collaboration of SATB2 with ATF4 and Runx2, we performed coimmunoprecipitations with extracts from 293 cells that had been transiently transfected with FLAG epitope-tagged SATB2 and various deletion constructs of Runx2 and ATF4 (Figures 7A and 7B). Immunoprecipitations with an anti-FLAG antibody and subsequent immunoblot analysis with an anti-Runx2 antibody directed against amino-terminal sequences indicated that Runx2 and various C-terminal deletions are efficiently coimmunoprecipitated with FLAG-SATB2 (Figure 7A). To examine the effects of the deletion of the amino-terminal sequences of Runx2, we used His-tagged Runx2 constructs and found that the same region that mediates the functional collaboration with SATB2 is also required for coimmunoprecipitation (Figure 7A). Likewise, we also detected efficient coimmunoprecipitation of Myc-tagged and endogenous ATF4 with anti-FLAG antibody (Figure 7B). In this experiment, we could detect coimmunoprecipitation of the amino-terminal 200 residues of ATF4 (Figure 7B, lower panel) and failed to coimmunoprecipitate the C-terminal residues (Figure 7B, upper panel). To determine whether the interactions of SATB2 with ATF4 and Runx2 are based on direct physical association, we performed His- and GST-pulldown experiments with purified recombinant proteins (Figure 7C). These experiments indicated that immobilized SATB2 could efficiently interact with ATF4, and reciprocal associations of SATB2 were detected with both ATF4 and Runx2. Taken together, these data show that SATB2 can physically interact with both ATF4 and Runx2, resulting in enhanced DNA binding and transactivation by these transcription factors.

To confirm the functional importance of the interactions detailed above in vivo, we examined whether the *Satb2*, *Runx2*, and *Atf4* genes interact genetically. We crossed *Satb2*^{+/-} and *Atf4*^{+/-} mice and analyzed bone

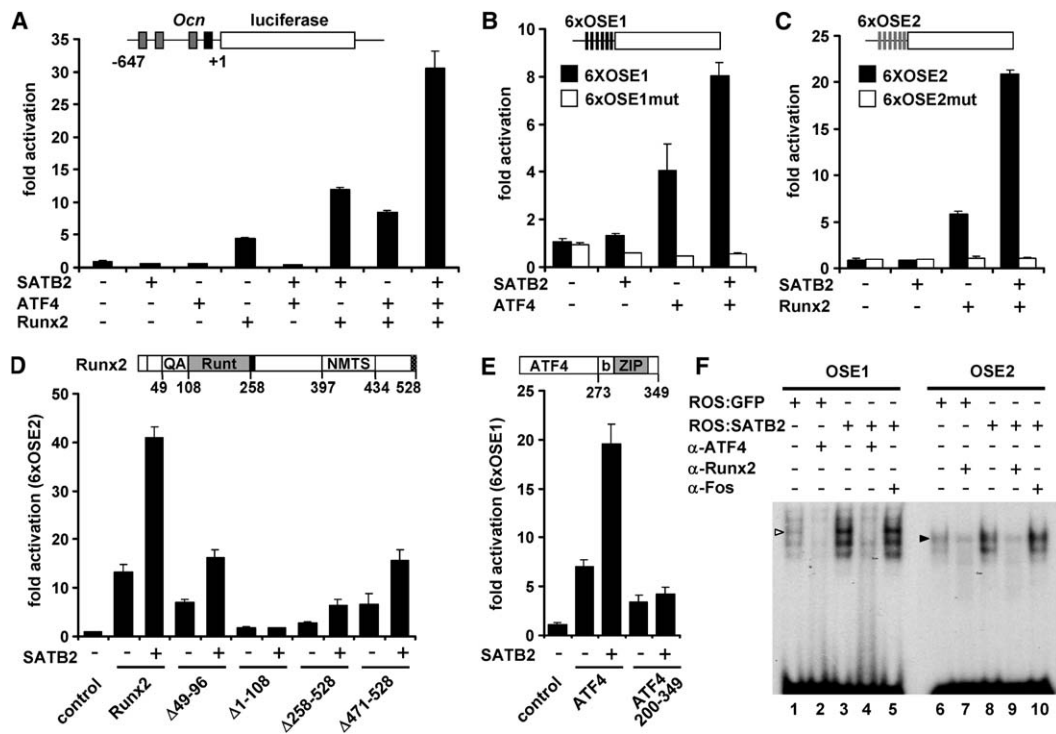


Figure 6. Functional Collaboration of SATB2 with ATF4 and Runx2

(A) COS7 cells were transiently transfected with a luciferase reporter construct containing a 647bp *Ocn* promoter fragment alone or together with SATB2, Runx2, and ATF4 expression plasmids in various combinations. The luciferase levels were normalized for the β -galactosidase activity of a cotransfected RSV-*lacZ* reporter and presented as fold activation relative to the luciferase levels of the *Ocn* reporter construct alone.

(B and C) COS7 cells were cotransfected with a luciferase reporter containing multimerized wild-type or mutated OSE1 (B) or OSE2 (C) sites alone or together with SATB2, ATF4, and Runx2 expression plasmids.

(D) Mapping of the SATB2 interaction domain in Runx2 by transfection of COS7 cells with SATB2 and different deletion mutants of Runx2.

(E) SATB2 functionally interacts with the N-terminal part of ATF4. COS7 cells were cotransfected with an OSE1-luciferase reporter together with SATB2 and ATF4 constructs. Error bars in (A), (B), (C), (D), and (E) represent the standard deviation of duplicate transfections.

(F) SATB2 enhances the binding of ATF4 and Runx2 to their respective binding sites. EMSA of nuclear extracts (2 μ g) from ROS17 osteosarcoma cells infected with either GFP- or SATB2-expressing retroviruses to detect binding of ATF4 and Runx2 to OSE1 (lanes 1–5) and OSE2 (lanes 6–10) oligonucleotides, respectively. Sp1 binding served as a control for the quality and quantity of the extracts (not shown). The identity of the protein:DNA complexes was confirmed by their reactivity with anti-ATF4 or anti-Runx2 antibodies. Anti-Fos antibody was used as a negative control.

development by van Gieson staining of E15.5 long bones. *Satb2*^{+/-} and *Atf4*^{+/-} bones showed normal formation of trabeculae and collagen fibrils, whereas double heterozygous bones displayed a marked reduction of bone formation (Figure 7D). Van Gieson staining of E17.5 long bones of *Satb2*/*Runx2* double heterozygous and single heterozygous embryos revealed a significant bone defect in the double heterozygotes, which was further corroborated by micro-CT analysis of vertebrae at birth (Figures 7E and 7F). The bone volume/total volume was reduced from 15.51% in wild-type mice to 3.53% in *Satb2*^{+/-}*Runx2*^{+/-} mice and 8.53% in *Satb2*^{+/-}*Atf4*^{+/-} mice. Moreover, the trabecular numbers/mm were reduced from 4.54 in wild-type mice to 0.79 in *Satb2*^{+/-}*Runx2*^{+/-} mice and 2.48 in *Satb2*^{+/-}*Atf4*^{+/-} mice. Finally, we examined whether the genetic interaction of SATB2 with Runx2 could have a role in early stages of osteoblast differentiation. Indeed, in situ hybridization of *Satb2* and *Runx2* single and double heterozygous E15.5 bones to detect transcripts of the

early molecular markers of bone formation, *Osx* and *AP*, showed a significant decrease in compound heterozygous embryos. Thus, *Satb2* interacts genetically with both *Atf4* and *Runx2* (Figure 7E).

DISCUSSION

Regulation of Craniofacial Patterning by SATB2

In the developing mouse, starting at E8.5, *Satb2* is expressed in the rhombomere region, at E9.0 in the first branchial arch, and subsequently in the medial parts of all four branchial arches that give rise to various facial structures of the adult (Hunt and Krumlauf, 1991; Bronner-Fraser, 1993; Köntges and Lumsden, 1996). Consistent with this expression pattern, *Satb2*^{+/-} embryos show multiple craniofacial defects that include a significant truncation of the mandible, a shortening of the nasal and maxillary bones, malformations of the hyoid bone, and a cleft palate. By analyzing the expression of several

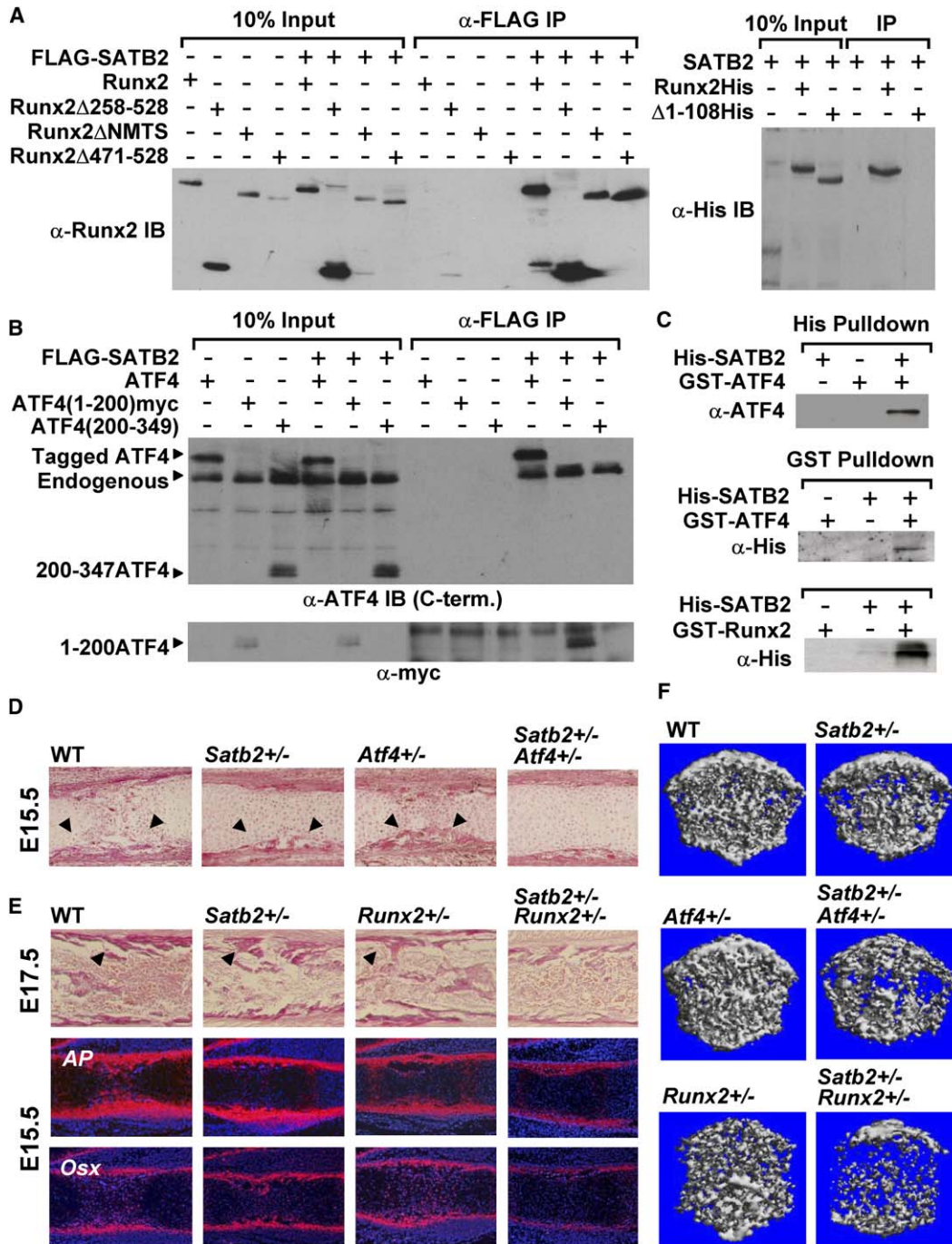


Figure 7. Physical and Genetic Interactions of SATB2 with ATF4 and Runx2

(A) Coimmunoprecipitation of Runx2 with FLAG-SATB2 in transiently transfected 293 cells. Immunoprecipitation (IP) was performed with an anti-FLAG antibody, and Runx2 proteins were detected by immunoblot (IB) analysis with anti-Runx2 (generated against the N terminus) or anti-His antibodies.

(B) Coimmunoprecipitation of ATF4 with FLAG-SATB2 in transfected 293 cells. ATF4 proteins were detected by immunoblot analysis with anti-ATF4 (generated against the C terminus) (upper panel) or anti-myc antibodies (lower panel). To increase the endogenous protein levels of ATF4, cells were treated with MG115.

(C) SATB2 binds directly to Runx2 and ATF4 in a His-tag pull-down with nickel beads (upper panel) or GST pull-down with glutathione beads (middle and lower panels).

(D) Van Gieson staining of collagen fibrils in E15.5 bones of wild-type (WT), *Satb2*, *Atf4* single, and double heterozygous mice. Trabeculae along the bone collar were detected in wild-type, *Satb2*^{+/-}, and *Atf4*^{+/-} bones (arrowheads) but not in the compound mutant.

genes implicated in craniofacial development, we identified *Lhx7* and several *Hox* genes as potential target genes for SATB2. Targeted inactivation of *Lhx7*, also termed *Lhx8*, results in a defect in the fusion of the palatal shelves but does not impair the development of other oral structures that are affected in *Satb2*^{-/-} embryos (Zhao et al., 1999). Moreover, mice homozygous for a null mutation of the *Msx1* gene, which has an altered pattern of expression in *Satb2*^{-/-} embryos, display a cleft palate (Satokata and Maas, 1994). The function of SATB2 in regulating palatogenesis is probably conserved during evolution as humans carrying deletions and balanced translocations involving chromosome 2q32-q33, which includes the *SATB2* locus, show a failed fusion of the secondary palate, which is also observed in *Satb2*^{-/-} mice (FitzPatrick et al., 2003).

Targeted inactivation of *Hoxa2*, which is expressed in the epithelium of rhombomere r2 and in the migrating neural crest of r4, results in the transformation of second arch-specific skeletal elements into first arch-specific elements (Gendron-Maguire et al., 1993; Rijli et al., 1993). The structures altered in *Hoxa2*^{-/-} embryos appear to be normal in *Satb2*^{-/-} mice and, therefore, we consider it likely that additional SATB2-regulated genes contribute to the craniofacial defects in *Satb2*^{-/-} embryos.

Regulation of *Hoxa2* by SATB2 in the Osteoblast Lineage

Beside defects in branchial arch patterning, *Hoxa2*^{-/-} mice show an upregulation of the cartilage- and bone-specifying genes *Sox9* and *Runx2* (Kanzler et al., 1998). Consistent with a function of *Hoxa2* in antagonizing bone formation, transgenic overexpression of *Hoxa2* in dermal bone precursors of the craniofacial area inhibits the formation of dermal bones, and the loss of *Hox* gene expression in cultured trunk neural crest cells correlates with the adoption of a skeletogenic fate (Kanzler et al., 1998; Creuzet et al., 2002). Interestingly, we detect an ectopic upregulation of *Hoxa2* in the forming calvarial bones of *Satb2*^{-/-} embryos at E15.5, and we could confirm the upregulation of *Hoxa2* and *Hoxb2* by quantitative RT-PCR assays with RNA from sorted osteoblasts (Figures 4B and 4C). Moreover, the rescue of the calvarial bone formation defect in *Satb2*^{-/-}*Hoxa2*^{-/-} mice suggests that the repression of *Hoxa2* by SATB2 is important for normal osteoblast differentiation.

The regulation of *Hoxa2* has been studied extensively and shown to involve distinct *cis*-acting elements that mediate expression in the hindbrain and in neural crest cells (Tumpel et al., 2002). In particular, an enhancer in the 3' region of the *Hoxa2* gene, which has been implicated in autoregulation, has been found to direct *LacZ* expression in r2 and rostral somites (Frasch et al., 1995; Lampe et al.,

2004). In vivo and in vitro, we detected binding of SATB2 to a sequence of the E11 enhancer that has the hallmarks of a MAR. A similar sequence is also found at the 3' end of the *Hoxb2* gene that is bound by SATB2 as determined in ChIP experiments (unpublished observation). Moreover, we show that the activity of the *Hoxa2* E11 enhancer can be repressed by SATB2 in transfected osteoblasts, and we find that deletion of the MAR region in the context of a *Hoxa2* transgene can result in the ectopic expression in regions that are positive for SATB2 expression in wild-type embryos. Taken together, our data suggest that SATB2 plays a role in downregulating *Hoxa2* expression in osteoblasts.

Regulation of Osteoblast Differentiation and Function by SATB2

During skeletogenesis, the function of SATB2 is not restricted to the patterning of the craniofacial region. Indeed, later stages of *Satb2*^{-/-} embryos show a delay in bone formation as characterized by a virtual absence of collagen deposition in E15.5 embryos. We also observed a marked decrease in the terminal differentiation of *Satb2*^{-/-} osteoblasts, as determined by an absence of *Bsp* and *Osn* expression. The similarity between the osteoblast phenotype of *Satb2*^{-/-} and *Atf4*^{-/-} mice suggested that the two proteins may interact physically and/or functionally with each other. Indeed, our molecular and genetic analysis indicated that *Satb2* interacts not only with ATF4 but also with Runx2. SATB2 can physically interact with both ATF4 and Runx2 and enhance the transactivation function of both proteins. Importantly, the same regions of ATF4 and Runx2 that mediate the functional synergy are also involved in the physical association with SATB2. The interaction of SATB2 with ATF4 and Runx2 augment their binding to the cognate DNA-recognition elements, although SATB2 does not bind itself to the OSE1 and OSE2 sequences. However, this mode of action of SATB2 does not exclude the possibility that it can function as a DNA bound protein. SATB2 has been shown to recognize specific sequences, termed MAR sequences (Dobrev et al., 2003), and indeed, SATB2 was found to regulate the *Bsp* promoter by binding to a site that resembles a bona fide MAR element. Moreover, SATB2 represses *Hoxa2* expression in osteoblasts through direct recognition of a MAR-like sequence. Therefore, SATB2 may act both as a transcriptional regulator that binds to specific DNA sequences and as a "scaffolding" protein that recruits other DNA bound proteins to specific subnuclear sites. This potentially dual function of SATB2 may also explain why *Atf4*^{-/-} mice have defects that resemble some but not all defects found in *Satb2*^{-/-} mice. Finally and more importantly, *Satb2* interact genetically with both *Atf4* and *Runx2* as the double heterozygous

(E) Top panel: Van Gieson staining of long bones of E17.5 *Satb2*, *Runx2* single and double heterozygous mice shows a virtual absence of trabeculae (arrowheads) in the double heterozygote. Middle and bottom panels: In situ hybridizations to detect transcripts of *alkaline phosphatase* (*AP*) and *Osterix* (*Osx*) in E15.5 wild-type, *Satb2*^{+/-}, *Runx2*^{+/-}, and *Satb2*^{+/-} *Runx2*^{+/-} tibias.

(F) Micro-CT analysis on vertebrae from P0 wild-type, *Satb2*^{+/-}, *Atf4*^{+/-}, *Runx2*^{+/-}, *Satb2*^{+/-} *Atf4*^{+/-}, and *Satb2*^{+/-} *Runx2*^{+/-} mice.

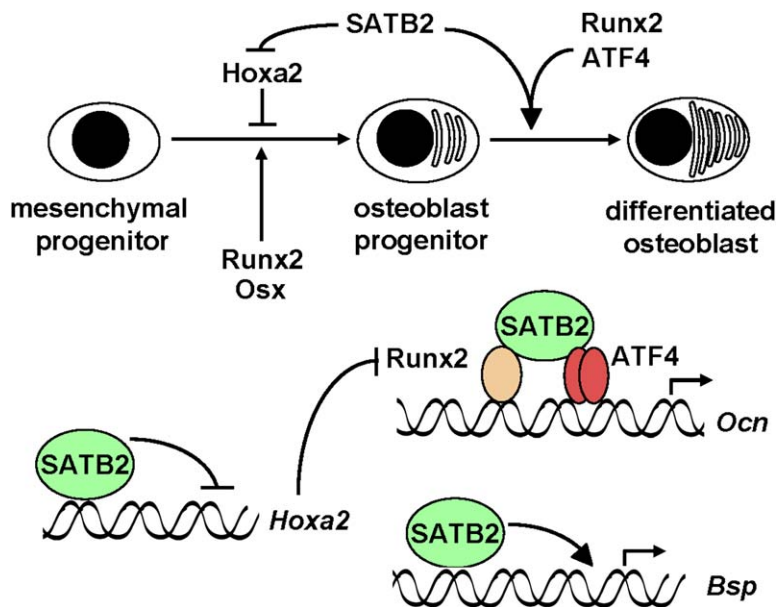


Figure 8. Model for a Transcriptional Network in Skeletal Development, in Which SATB2 Regulates This Process by Repressing *Hoxa2* and Augmenting the Functions of the Osteoblast Determinants Runx2 and ATF4

SATB2 can activate or repress gene transcription by direct binding to DNA, and it can act as a scaffold that enhances the activity of other DNA binding proteins.

mutant mice display a severe defect in bone development, which is not observed in single heterozygous mutant mice. Our molecular and genetic analysis also indicated that the interaction of SATB2 with Runx2 may be functionally even more important than the interaction with ATF4 because *Satb2*^{+/-}*Runx*^{+/-} embryos have a more severe osteoporotic phenotype than *Satb2*^{+/-}*Atf4*^{+/-} embryos. In addition, many genes that are deregulated in *Satb2*^{-/-} osteoblasts are known targets of Runx2.

Previous analysis of the *osteocalcin* promoter, a well-studied model for osteoblast-specific gene expression, has indicated that Runx2 and ATF4 synergize via nonadjacent binding sites (Xiao et al., 2005). As ATF4 and Runx2 do not interact directly, it has been proposed that an additional protein mediates the functional synergy between these transcription factors. Our findings that SATB2 interacts with both Runx2 and ATF4 and augments their synergistic activation suggest that SATB2 may act to couple these osteoblast-specific transcription factors. Although this interaction enhances the binding of ATF4 and Runx2 to the *osteocalcin* promoter in vitro, this effect is modest and cannot explain the marked functional synergy. Therefore, SATB2 may participate in recruitment of proteins to specific subnuclear sites. Runx2 has been originally identified as NMP2, an osteoblast-specific MAR binding protein that associates with the nuclear matrix via a C-terminal targeting sequence and acts as a scaffold that targets regulatory factors and gene sequences to specific subnuclear sites (Bidwell et al., 1993; Choi et al., 2001; Zaidi et al., 2005). However, SATB2 interacts with the amino-terminal domain of Runx2, which is also required for the functional synergy of Runx2 with ATF4. Moreover, SATB2 does not appear to mediate subnuclear targeting of Runx2, as the punctate nuclear distribution of Runx2 is not altered in *Satb2*^{-/-} osteoblasts (data not shown).

Therefore, we favor the view that SATB2 may act to recruit ATF4 to Runx2 multiprotein complexes in osteoblasts.

In conclusion, SATB2 is an unusual molecular determinant of skeletal development. It can act not only as an activating or repressing DNA bound protein but also as a protein scaffold that enhances the activity of other DNA binding proteins (Figure 8). By its ability to regulate the expression or activity of multiple key determinants of skeletal development, SATB2 appears to represent a molecular node of a transcriptional network underlying this process.

EXPERIMENTAL PROCEDURES

Satb2 Gene Targeting

A β -galactosidase/pGKneo-pA cassette was inserted in frame with the ATG codon of the SATB2 gene. Homologous recombination was identified by Southern blot analysis with 5' internal and 3' external probes. Embryos were genotyped by PCR on DNA obtained from the yolk sacs or tail biopsies. Primer sequences for amplifying the homology arms of the targeting construct and for genotyping are provided upon request.

Morphological Analysis and In Situ Hybridization

For skeletal preparation, embryos were fixed in 95% ethanol. Alcian Blue/Alizarin Red staining was performed according to standard protocols. For histological analysis, embryos were fixed with 4% paraformaldehyde, embedded in paraffin, sectioned in 7 μ m thick slices, and stained with hematoxylin/eosin, von Kossa, and van Gieson reagents according to standard protocols. The micro-CT analysis was performed using the μ CT40 Scanner according to the standard criteria (Valentin et al. 2003). LacZ staining and in situ hybridizations were performed on 20 μ m thick cryosections. For detailed information, see Supplemental Experimental Procedures.

Cell Culture, Transient Transfections, and Reporter Assays

Primary osteoblasts were isolated from E18.5 embryos essentially as described (Ducy and Karsenty, 1995). C2C12 and COS7 cells were grown in α -MEM supplemented with 10% fetal bovine serum.

Transient transfections were performed using Lipofectamine (invitrogen) according to the manufacturer's instructions.

Protein Expression, Pull-Down Assays, EMSA, Immunoprecipitation, and Immunoblot Analysis

Recombinant proteins were expressed and purified, and pull-down assays were performed as previously described (Dobrev et al., 2003; Yang et al., 2004). EMSA, coimmunoprecipitation, and chromatin immunoprecipitations were performed as described (Dobrev et al., 2003). For oligonucleotides and primers, see [Supplemental Experimental Procedures](#). For immunoblot analysis, antibodies were used in the following dilutions: anti-His (Santa Cruz) 1:1000; anti-ATF4 (Santa Cruz) 1:500; anti-Runx2 1:2000; and anti- β galactosidase 1:5000.

RNA Isolation, RT-PCR, and Real-Time PCR

RNA was isolated using the Trizol reagent. Real-time PCR was performed with SYBR GREEN PCR master mix (Applied Biosystems) using the ABI PRISM 7000 sequence detection system. The cycle numbers were normalized to β -actin. Primer pairs are described in [Supplemental Experimental Procedures](#).

FDG Loading and FACS Sorting

For the sorting of SATB2-LacZ positive cells, osteoblasts were loaded with fluorescein digalactoside (Molecular Probes) using hypotonic shock according to the manufacturer's instructions. After FDG loading, the cells were kept on ice for 30 min before FACS sorting and sorted on a Vantage cell sorter using the CellQuest software.

Supplemental Data

Supplemental Data include five figures and Experimental Procedures and can be found with this article online at <http://www.cell.com/cgi/content/full/125/5/971/DC1/>.

ACKNOWLEDGMENTS

We thank Drs. A. Gründer, M. Kieslinger, W. Roth, A. Neubüser, N. Bobola, M. Feuring-Buske, and C. Bleul for discussions and advice. We are grateful to Drs. F. Rijli and E. Wagner for discussions and helpful suggestions. We thank Drs. T. Lufkin and T. Gridley for plasmids and *Hoxa2*^{-/-} mice, respectively. This work was supported by funds of the Max Planck Society and the DFG to R.G.I.F. is funded by the Spanish Ministerios de Educación y Ciencias y de Sanidad.

Received: November 1, 2005

Revised: March 13, 2006

Accepted: May 2, 2006

Published: June 1, 2006

REFERENCES

- Alvarez, J.D., Yasui, D.H., Niida, H., Joh, T., Loh, D.Y., and Kohwi-Shigematsu, T. (2000). The MAR-binding protein SATB1 orchestrates temporal and spatial expression of multiple genes during T-cell development. *Genes Dev.* *14*, 521–535.
- Benson, M.D., Bargeon, J.L., Xiao, G., Thomas, P.E., Kim, A., Cui, Y., and Franceschi, R.T. (2000). Identification of a homeodomain binding element in the bone sialoprotein gene promoter that is required for its osteoblast-selective expression. *J. Biol. Chem.* *275*, 13907–13917.
- Bidwell, J.P., Van Wijnen, A.J., Fey, E.G., Dworetzky, S., Penman, S., Stein, J.L., Lian, J.B., and Stein, G.S. (1993). Osteocalcin gene promoter-binding factors are tissue-specific nuclear matrix components. *Proc. Natl. Acad. Sci. USA* *90*, 3162–3166.
- Bode, J., Benham, C., Knopp, A., and Mielke, C. (2000). Transcriptional augmentation: modulation of gene expression by scaffold/matrix-attached regions (S/MAR elements). *Crit. Rev. Eukaryot. Gene Expr.* *10*, 73–90.
- Britanova, O., Akopov, S., Lukyanov, S., Gruss, P., and Tarabykur, V. (2005). Novel transcription factor Sat62 interacts with matrix attachment region DNA elements in a tissue-specific manner and demonstrates cell-type-dependent expression in the developing mouse CNS. *Eur. J. Neurosci.* *27*, 658–668.
- Bronner-Fraser, M. (1993). Neural crest cell migration in the developing embryo. *Trends Cell Biol.* *3*, 392–397.
- Cai, S., Han, H.J., and Kohwi-Shigematsu, T. (2003). Tissue-specific nuclear architecture and gene expression regulated by SATB1. *Nat. Genet.* *34*, 42–51.
- Choi, J.Y., Pratap, J., Javed, A., Zaidi, S.K., Xing, L., Balint, E., Dalamangas, S., Boyce, B., van Wijnen, A.J., Lian, J.B., et al. (2001). Subnuclear targeting of Runx/Cbfa/AML factors is essential for tissue-specific differentiation during embryonic development. *Proc. Natl. Acad. Sci. USA* *98*, 8650–8655.
- Chiaska, O., Musci, T., and Capecci, M.M. (1992). Developmental defects of the ear, cranial nerves and hindbrain resulting from targeted disruption of the mouse homeobox gene *Hox-1.6*. *Nature* *355*, 516–520.
- Cockerill, P.N., and Garrard, W.T. (1986). Chromosomal loop anchorage of the kappa immunoglobulin gene occurs next to the enhancer in a region containing topoisomerase II sites. *Cell* *144*, 273–282.
- Creuzet, S., Couly, G., Vincent, C., and Le Douarin, N.M. (2002). Negative effect of Hox gene expression on the development of the neural crest-derived facial skeleton. *Development* *129*, 4301–4313.
- de Crombrugge, B., Lefebvre, V., and Nakashima, K. (2001). Regulatory mechanisms in the pathways of cartilage and bone formation. *Curr. Opin. Cell Biol.* *13*, 721–727.
- Depew, M.J., Lufkin, T., and Rubenstein, J.L. (2002). Specification of jaw subdivisions by *Dlx* genes. *Science* *298*, 381–385.
- Dobrev, G., Dambacher, J., and Grosschedl, R. (2003). SUMO modification of a novel MAR-binding protein, SATB2, modulates immunoglobulin mu gene expression. *Genes Dev.* *17*, 3048–3061.
- Ducy, P., and Karsenty, G. (1995). Two distinct osteoblast-specific cis-acting elements control expression of a mouse osteocalcin gene. *Mol. Cell. Biol.* *15*, 1858–1869.
- Fitzpatrick, D.R., Carr, I.M., McLaren, L., Leek, J.P., Wightman, P., Williamson, K., Gautier, P., McGill, N., et al. (2003). Identification of SATB2 as the cleft palate gene on 2q32–q33. *Hum. Mol. Genet.* *12*, 2491–2501.
- Frasch, M., Chen, X., and Lufkin, T. (1995). Evolutionary-conserved enhancers direct region-specific expression of the murine *Hoxa-1* and *Hoxa-2* loci in both mice and *Drosophila*. *Development* *121*, 957–974.
- Gasser, S.M., and Laemmli, U. (1986). Cohabitation of scaffold binding regions with upstream/enhancer elements of three developmentally regulated genes of *D. melanogaster*. *Cell* *46*, 521–530.
- Gendron-Maguire, M., Mallo, M., Zhang, M., and Gridley, T. (1993). *Hoxa-2* mutant mice exhibit homeotic transformation of skeletal elements derived from cranial neural crest. *Cell* *75*, 1317–1331.
- Graham, A., and Smith, A. (2001). Patterning the pharyngeal arches. *Bioessays* *23*, 54–61.
- Hunt, P., and Krumlauf, R. (1991). Deciphering the Hox code: clues to patterning branchial regions of the head. *Cell* *66*, 1075–1078.
- Jenuwein, T., Forrester, W.C., Fernandez-Herrero, L.A., Laible, G., Dull, M., and Grosschedl, R. (1997). Extension of chromatin accessibility by nuclear matrix attachment regions. *Nature* *385*, 269–272.
- Kanzler, B., Kuschert, S.J., Liu, Y.H., and Mallo, M. (1998). *Hoxa-2* restricts the chondrogenic domain and inhibits bone formation during development of the branchial area. *Development* *125*, 2587–2597.

- Köntges, G., and Lumsden, A. (1996). Rhombencephalic neural crest segmentation is preserved throughout craniofacial ontogeny. *Development* *122*, 3229–3242.
- Kohwi-Shigematsu, T., Maass, K., and Bode, J. (1997). A thymocyte factor SATB1 suppresses transcription of stably integrated matrix-attachment region-linked reporter genes. *Biochemistry* *36*, 12005–12010.
- Lampe, X., Picard, J.J., and Rezsóhazy, R. (2004). The Hoxa2 enhancer 2 contains a critical Hoxa2 responsive regulatory element. *Biochem. Biophys. Res. Commun.* *316*, 898–902.
- Mariani, F.V., and Martin, G.R. (2003). Deciphering skeletal patterning: clues from the limb. *Nature* *423*, 319–325.
- Namciu, S.J., Friedman, R.D., Marsden, M.D., Sarausad, L.M., Jasoni, C.L., and Fournier, R.E. (2004). Sequence organization and matrix attachment regions of the human serine protease inhibitor gene cluster at 14q32.1. *Mamm. Genome* *15*, 162–178.
- Nakashima, K., Zhou, X., Kunkel, G., Zhang, Z., Deng, J.M., Behringer, R.R., and de Crombrughe, B. (2002). The novel zinc finger-containing transcription factor osterix is required for osteoblast differentiation and bone formation. *Cell* *108*, 17–29.
- Olsen, B.R., Reginato, A.M., and Wang, W. (2000). Bone development. *Annu. Rev. Cell Dev. Biol.* *16*, 191–220.
- Rijli, F.M., Mark, M., Lakkaraju, S., Dierich, A., Dolle, P., and Chambon, P. (1993). A homeotic transformation is generated in the rostral branchial region of the head by disruption of Hoxa-2, which acts as a selector gene. *Cell* *75*, 1333–1349.
- Santagati, F., and Rijli, F.M. (2003). Cranial neural crest and the building of the vertebrate head. *Nat. Rev. Neurosci.* *4*, 806–818.
- Satokata, I., and Maas, R. (1994). Mx1 deficient mice exhibit cleft palate and abnormalities of craniofacial and tooth development. *Nat. Genet.* *6*, 348–356.
- Trainor, P.A., and Krumlauf, R. (2001). Hox genes, neural crest cells and branchial arch patterning. *Curr. Opin. Cell Biol.* *13*, 698–705.
- Tumpel, S., Maconochie, M., Wiedemann, L.M., and Krumlauf, R. (2002). Conservation and diversity in the cis-regulatory networks that integrate information controlling expression of Hoxa2 in hindbrain and cranial neural crest cells in vertebrates. *Dev. Biol.* *246*, 45–56.
- Valentin, D., Laroche, N., Boudignon, B., Lafage-Proust, M., Christian, A., Rueggsegger, P., and Vicoi, L. (2003). Noninvasive in vivo monitoring of bone architecture alterations in hindlimb-unloaded female rats using novel three-dimensional microcomputed tomography. *J. Bone Miner. Res. J. Bone Miner. Res.* *18*, 1622–1631.
- Veitch, E., Begbie, J., Schilling, T.F., Smith, M.M., and Graham, A. (1999). Pharyngeal arch patterning in the absence of neural crest. *Curr. Biol.* *9*, 1481–1484.
- Xiao, G., Jiang, D., Ge, C., Zhao, Z., Lai, Y., Boules, H., Phimpilai, M., Yang, X., et al. (2005). Cooperative interactions between activating transcription factor 4 and Runx2/Cbfa1 stimulate osteoblast-specific osteocalcin gene expression. *J. Biol. Chem.* *280*, 30689–30696.
- Yang, X., and Karsenty, G. (2004). ATF4, the osteoblast accumulation of which is determined post-translationally, can induce osteoblast-specific gene expression in non-osteoblastic cells. *J. Biol. Chem.* *279*, 47109–47114.
- Yang, X., Matsuda, K., Bialek, P., Jacquot, S., Masuoka, H., Schinke, T., Li, L., Brancorsini, S., et al. (2004). ATF4 is a substrate of RSK2 and an essential regulator of osteoblast biology; implication for Coffin-Lowry Syndrome. *Cell* *117*, 387–398.
- Yasui, D., Miyano, M., Cai, S., Varga-Weisz, P., and Kohwi-Shigematsu, T. (2002). SATB1 targets chromatin remodelling to regulate genes over long distances. *Nature* *419*, 641–645.
- Zaidi, S.K., Young, D.W., Choi, J.-Y., Pratap, J., Javed, A., Montecino, M., Stein, J.L., van Wijnen, A.J., et al. (2005). The dynamic organization of gene-regulatory machinery in nuclear microenvironments. *EMBO Reports* *6*, 128–133.
- Zhao, Y., Guo, Y.J., Tomac, A.C., Taylor, N., Grinberg, A., Lee, E.J., Huang, S., and Westphal, H. (1999). Isolated cleft palate in mice with a targeted mutation of the LIM homeobox gene *lhx8*. *Proc. Natl. Acad. Sci. USA* *96*, 15002–15006.